JQS Journal of Quaternary Science

QRA Quaternary Research Association

High-resolution chronology of 24 000-year long cores from two lakes in the Polar Urals, Russia, correlated with palaeomagnetic inclination records with a distinct event about 20 000 years ago

HAFLIDI HAFLIDASON,* [iD] JO BRENDRYEN, [iD] REIDUN F. ELDEGARD, JAN MANGERUD, SÆDIS ÓLAFSDÓTTIR, CARL REGNÉLL [iD] and JOHN INGE SVENDSEN [iD]
Department of Earth Science and Bjerknes Centre for Climate Research, University of Bergen, Allegt. 41, Bergen, 5007, Norway

ABSTRACT: Based on radiocarbon dating, a tephra horizon, varve counts and palaeomagnetism, detailed age models covering the last ~24 k cal a BP, have been developed for the stratigraphy in the lakes Bolshoye Shchuchye and Maloye Shchuchye in the Polar Ural Mountains, Russia. The inclination curves from these lakes show nearly identical palaeomagnetic secular variations in the studied cores from both lakes, allowing for a precise correlation between the cores. A large and very distinct inclination deviation, named the Bolshoye Shchuchye Event, was identified in all cores retrieved from both lakes. It lasted over a period of 1245 years, from 20 470 to 19 225 cal a BP. The well-dated palaeomagnetic inclination graph offers a new possibility to correlate archives in this part of the Arctic for the last ~24 k cal a BP, probably also over longer distances. The sedimentation rate shows the same trend in all cores from both lakes, including high input during the Last Glacial Maximum and gradually lowering after ~18 k cal a BP to lower and stable Holocene values.
© 2021 The Authors. *Journal of Quaternary Science* Published by John Wiley & Sons Ltd.

KEYWORDS: chronology; inclination; Polar Ural Mountains; sedimentation rate

Introduction

Establishing an accurate and robust chronological framework for Arctic/Polar lake records is often challenging due to the low content of material suitable for radiocarbon dating and commonly low sedimentation rates (e.g. Colman *et al.*, 1996; Saarnisto and Saarinen, 2001; Henriksen *et al.*, 2008; Alexanderson *et al.*, 2014; Vyse *et al.*, 2020; Gromig *et al.*, 2019, 2021). Large areas were also covered by ice sheets during the Last Glacial Maximum (LGM) and only a few lakes have preserved records reaching beyond ~15 k cal a BP (e.g. Hughes *et al.*, 2016). The discovery of the high-resolution core records in Lake Bolshoye Shchuchye (hereafter abbreviated to Bol. Shchuchye), reaching back into the LGM in the Polar Ural Mountains in Arctic Russia (Fig. 1) (Svendsen *et al.*, 2019), has, however, offered opportunities to study in great detail the palaeoclimatic, environmental and vegetational history of this region since the peak of the LGM (Bjune *et al.*, 2021; Cowling *et al.*, 2021; Clark *et al.*, 2019; Clarke *et al.*, 2020; Lammers *et al.*, 2019; Lenz *et al.*, 2021; Regnéll *et al.*, 2019; Svendsen *et al.*, 2019). To maximise the utility of such high-resolution proxy records a combination of several dating methods is needed in order to test the internal consistency of the obtained ages and in the end establish an accurate and robust age model.

The first chronological model established for Lake Bol. Shchuchye was based on 27 accelerator mass spectrometry (AMS) ^{14}C dates on plant remains (Svendsen *et al.*, 2019) in core 506-48, the well-dated marker horizon Vedde Ash

(Haflidason *et al.*, 2019b) and a long sequence of counted (annual) varves (Regnéll *et al.*, 2019). In the present study the age model has been improved by an additional 11 AMS ^{14}C dates on plant remains, a new statistical Bayesian age modelling, and a precise correlation between the cores by means of detailed palaeomagnetic records. This improved age model of core 506-48 has been applied in the companion papers by Bjune *et al.* (2021) and by Cowling *et al.* (2021) and will be used in future papers on this lake.

The high-resolution palaeomagnetic record for core 506-48 also offers an exceptional possibility for core-to-core correlation both within this lake and to more distal lakes, and since 506-48 is so well-dated it also provides a means for dating the correlated cores. In this study, we present only the inclination and the magnetic susceptibility records from the selected cores. The inclination curves from our three cores, and indeed core Co1321 (Lenz *et al.*, 2021), are almost identical and this result shows that the inclination record can stand alone for our correlation purposes. We note that interpretation of the inclination record is simpler than for the declination record because inclination needs no directional alignment between different core sections.

Like Lake Bol. Shchuchye, the second largest lake in the Polar Ural Mountains, Lake Maloye Shchuchye (hereafter abbreviated to Mal. Shchuchye), is also found to preserve a long and continuous sedimentary record (Eldegard, 2019) (Fig. 1). The high minerogenic content of the sediments in Lake Mal. Shchuchye has, however, made the dating of these sediments very challenging and inaccurate, especially beyond the Holocene (Eldegard, 2019). The few dating results available from the older strata in Lake Mal. Shchuchye indicated that this lake has also experienced sedimentation rates of 1–2 m ka[-1] as in core 506-48 in Lake Bol. Shchuchye

*Correspondence: H. Haflidason, as above.

E-mail: Haflidi.Haflidason@uib.no

Figure 1. A) Key map showing the northern Ural Mountains and the adjacent Arctic areas. The white shaded area marks the outline of the Scandinavian and the Barents Sea ice sheets during the Last Glacial Maximum (LGM), according to Svendsen *et al.* (2004). The black box over the northern Urals marks the outline of Fig. 1B. B) Overview map of the Polar Urals, with a white box showing the outline of the map in Fig. 1C. Letters B and M show locations of the lakes Bol. Shchuchye and Mal. Shchuchye. The blue star shows the location of the Lake Gerdizty discussed in Svendsen *et al.* (2014). C) Shaded topographic map of the study area. B – Lake Bolshoye Shchuchye, M – Lake Maloye Shchuchye. White dashed lines show the drainage area for each lake. Red dots and labels show the core locations and numbers, respectively. Black letters give the altitudes of some of the highest mountain peaks bordering the drainage areas. [Color figure can be viewed at wileyonlinelibrary.com]

(Eldegard 2019; Regnéll *et al.*, 2019; Svendsen *et al.*, 2019). If correct, the Polar Ural Mountains contain two long and continuous lake archives that provide continuous stratigraphical records of decadal resolution in two different types of lake setting. Thus, they offer a unique possibility to identify and evaluate details in leads and lags between climatic and/or environmental events on local and hemispheric scales.

The main aims of this paper are to present the palaeomagnetic results and to establish a statistically robust chronological model for a ~24 000-year long and continuous record from the two largest lakes of the Polar Ural Mountains. To evaluate the environmental changes in the study area since the peak of the LGM the general development in the sedimentation rate within these two lakes will also be assessed.

Geological setting

The lakes Bol. Shchuchye and Mal. Shchuchye are in the interior of the Polar Urals in valleys that are glacially incised into the 800–1000 m high mountains (Fig. 1). The northwest–southeast orientation of the lake basins is tectonically controlled from the Uralian Orogeny at 250–300 Ma (Puchkov, 1997). The bedrock of the eastern and northwestern mountain flanks of both lakes consists predominantly of Proterozoic–Cambrian basaltic and andesitic rocks, whereas the bedrock to the south and west consists of quartzite and phyllite rocks of Ordovician age (Dushin *et al.*, 2009) (Fig. 2);

(Svendsen *et al.*, 2019). Studies by Haflidason *et al.* (2019a) and Svendsen *et al.* (2019) revealed that the lake basin of Bol. Shchuchye remained ice-free during the LGM, but the surrounding mountain areas were occupied by restricted mountain glaciers.

Bol. Shchuchye (67°53.024′N, 66°18.036′E) is the largest and deepest lake in the Polar Ural Mountains; it is 12.8 km long, about 1 km wide (11.8 km²), 140 m deep, and with a lake level at 187 m asl. The mountain areas on both sides of the basin in the northwest make up the largest part of the catchment, covering an area of ~215 km² which is drained by the Pyriatanyu River. The drainage area along the southern end of the basin consists of narrow zones with small inflow streams. The outlet at the southern end of the lake flows over a bedrock sill into the Bol. Shchuchya River (Fig. 1).

Mal. Shchuchye (67°82′N, 66°16′E) is the second largest lake in the Polar Urals. It is located ~10 km to the west of Bol. Shchuchye at an altitude of 287 m asl (Fig. 1). The lake has a similar shape to Bol. Shchuchye, but is smaller and shallower, being 7.15 km long, and ~0.6 km wide (3.8 km²), and has a maximum water depth of ~40 m. The 51 km² catchment area covers the mountain areas in the southwest and in the northwest, but most of the run-off is drained through the Nyuya Pyryantanë River that flows into the northwestern end of the lake (Fig. 1). The hill slopes along the western and the eastern border of the lake are rather steep with small brooks from cirques or gullies (Fig. 1).
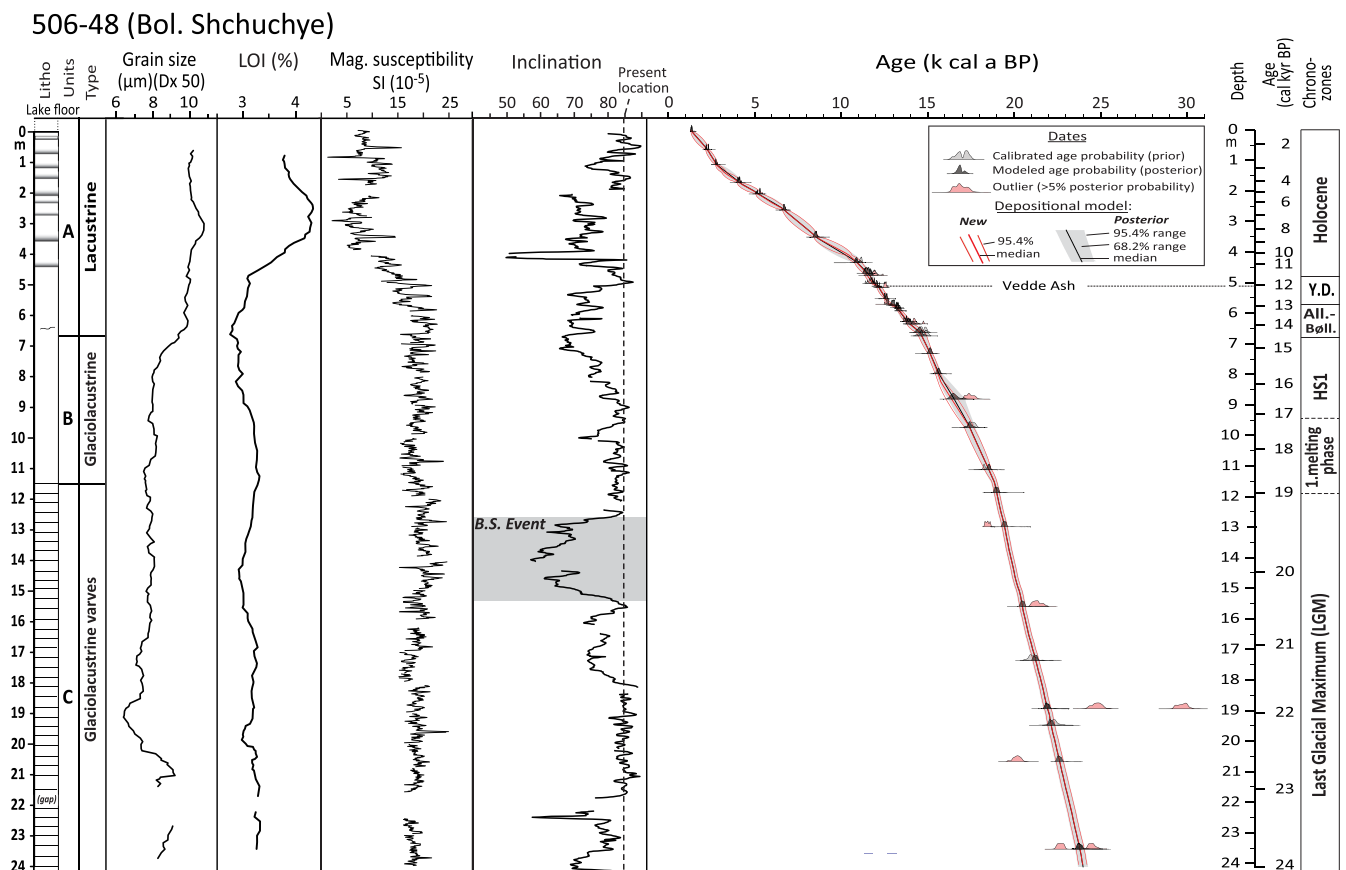
Figure 2. Lithological log of core 506‐48 from Bol. Shchuchye plotted on a linear depth scale. The time scale in calendar years and the chronozones for the recovered period are added to the right. The curves show the median grain size (D×50), loss on ignition (LOI), magnetic susceptibility, and palaeomagnetic inclination. The first order age model developed (posterior) is marked with a grey shaded area, but the final age model is in red with the median age as the thick line and the thin lines representing the 95% confidence interval. The vertical dashed line on the inclination graph marks the present‐day inclination of geomagnetic field in the lake area. The stratigraphical extent of the Bol. Shchuchye Event is marked as a grey shaded area. The boundary ages of the chronozones and the Heinrich Stadial 1 (HS1) listed follow Hodell *et al.* (2017) and Mangerud (2021). [Color figure can be viewed at wileyonlinelibrary.com]

Material and methods

Coring of the lake sediments

The coring campaign was conducted in 2009 in both lakes from ice applying an UWITEC Piston Corer equipped with 90 mm inner diameter PVC liner (Svendsen *et al.*, 2019). From Bol. Shchuchye the 24 m long sediment cores 506‐48 and 506‐50 were retrieved from 100 m water depth in the southern part of the lake (67°51.371′N, 66°21.502′E). To ensure full recovery of the sedimentary sequence of Bol. Shchuchye, the two cores were taken only 20 m apart from each other and with an overlap of 30–40 cm between each 2 m core segment (Svendsen *et al.*, 2019). For the deepest 4 m of the Bol. Shchuchye cores, 9 cm steel tubes were used instead of the PVC liners (Svendsen *et al.*, 2019). The 25.07 m long core 506‐51 from Mal. Shchuchye (67°49.10′N, 66°09.70′E) was retrieved from 30 m water depth in the central part of lake (Fig. 1). All the retrieved core segments were transported in sealed barrels (steel or PVC) to the laboratory at the University of Bergen and stored in the controlled cool storeroom before being subsampled.

Sampling, measurements and analyses

In Bergen, cores 506‐48, 506‐50 and 506‐51 were divided into 1 m long sections and split in half lengthwise. The colour and X‐ray fluorescence (XRF) logs performed on cores 506‐50 and 506‐48 identified a minor gap in sediment recovery between two sections of the key core 506‐48.

To correct for this gap, data from a 13 cm long interval in 506‐50 were spliced with core 506‐48 below the section break at 593 cm. The resulting composite depth scale and stratigraphic column are used in the age model. Details of how these two cores overlap is illustrated in Fig. 7 in Svendsen *et al.* (2019). All data and figures presented in this paper use the updated composite depth. The depth corrected inclination curves for the cores 506‐48 and 506‐50, located 20 m apart, are shown Fig. S1.

All cores were scanned for digital colour images, measured for bulk element analysis using an ITRAX XRF core scanner (Cox Analytical, Sweden), and lithologically logged for texture and structure before subsampling for sedimentological, biological and hydrological analyses (Bjune *et al.*, 2021; Clark *et al.*, 2019; Clarke *et al.*, 2020; Cowling *et al.*, 2021; Eldegard, 2019; Hovland, 2015; Regnéll *et al.*, 2019). The grain‐size analyses were carried out with 5–10 cm vertical intervals. The variation in sample intervals is due to turbidites, which were avoided. The analyses were performed using a Mastersizer 3000 laser diffraction instrument from Malvern Instruments Ltd connected to a Hydroseries wet dispersion unit (Eldegard, 2019; Regnéll *et al.*, 2019). The grain‐size data processing was carried out with the GRADISTAT v.8 program (Blott and Pyne, 2001). The percentage loss on ignition (LOI) was measured approximately every 10 cm in cores 506‐48 and 506‐51 following the procedure of Dean (1974) and Heiri *et al.* (2001). A simplified log of cores 506‐48 and 506‐51, with selected sedimentological parameters, is presented in Figs. 2 and 3.
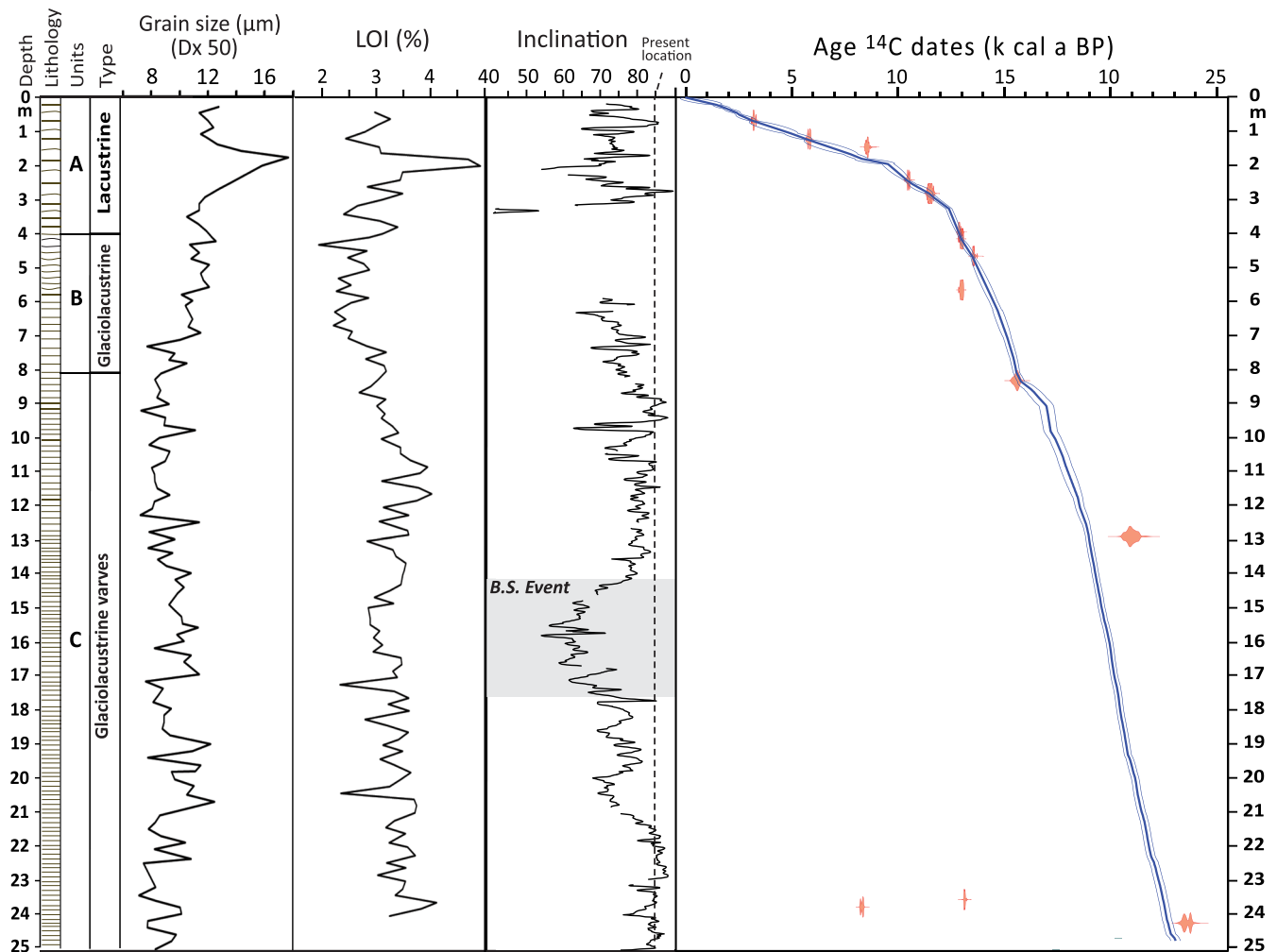
Figure 3. Lithological log of core 506-51 from Mal. Shchuchye plotted on a linear depth scale. The curves show the median grain size (D×50), loss on ignition (LOI), and palaeomagnetic inclination. The calibrated ^{14}C dates obtained from this core are plotted with the probability distribution. The median age of the calibrated model is represented by the thick line and the thin line represents the 95% confidence interval. The vertical dashed line on the inclination graph marks the present-day inclination of geomagnetic field in the lake area. The stratigraphical extent of the Bol. Shchuchye Event is marked with grey shaded area inside the inclination graph. [Color figure can be viewed at wileyonlinelibrary.com]

The sediments extracted for palaeomagnetic analyses from cores 506-48, 506-50 and 506-51 were sampled using u-channels with an inner diameter of 2 cm (Weeks *et al.*, 1993). The natural remanent magnetisation (NRM) of the u-channels was measured at 1 cm intervals using the 2 G Enterprises model 755-1.65UC 3-axis superconducting rock magnet-ometer optimised for u-channel samples at the Paleomagnetic and Environmental Magnetic Research Laboratory, College of Earth, Ocean, and Atmospheric Sciences, Oregon State University. The width of the response function of the magnetometer pick-up coils at ~7.5 cm (Oda and Xuan, 2014) is wider than earlier liquid He u-channel superconducting rock magnetometers versions (Weeks *et al.*, 1993). In spite of that, the enhanced symmetry of all three axes, improved coupling between the sample and the pick-up coils and the lack of negative lobes outside of the response function (Oda *et al.*, 2016) result in improved measurement accuracy (e.g. Roberts, 2006). The NRM measurement was followed by alternating field (AF) demagnetisation at 5–10 mT increments (10, 15, 20, 25, 30, 35, 40, 45, 50, 55, 60, 65, 70, 80, 90, 100 mT). For most of the cores 8–11 consecutive measurements after AF demagnetisation at peak fields between 10 and 70 mT were used. Only for the lowermost metre of core 506-51, the characteristic remanent magnetization (ChRM) was defined

between the 20 and 30 mT AF demagnetisation steps. Data affected by edge effects as, e.g., incompletely filled u-channels, or disturbed sediment either through sampling or coring, though minimal, were generally excluded from the data set.

Dating methods

Cores 506-48 and 506-50

The chronology of the key core 506-48 is based on 27 AMS radiocarbon (^{14}C) dates, the identification of the Vedde Ash (12.1 k cal a BP) and on counting of a floating sequence of 5000 annual laminations (varves) below 11.40 m, i.e. covering the lowermost 12.6 m of the core (Haflidason *et al.*, 2019b; Regnéll *et al.*, 2019; Svendsen *et al.*, 2019) (Fig. 2; Table 1). The ^{14}C sample extraction of terrestrial plant fragments and treatment procedure is provided by Svendsen *et al.* (2019). Due to the small size of the plant fragments, they could not be identified to their respective species name. The AMS ^{14}C samples were measured at the Poznań Radiocarbon Laboratory of the Adam Mickiewicz University, Beta Analytic, and the radiocarbon dating laboratory at Lund University (Table 1) and calibrated against the reference curves IntCal20 (Reimer

Table 1. The ¹⁴C dates, Vedde Ash tephra horizon and varve-count boundaries applied in the age model for core 506-48, Bol. Shchuchye. Dates that were not included in the final age model are marked with red letters. All ages are calibrated using the OxCal 4.4.1 software (Bronk Ramsey *et al.*, 2009a) with IntCal20 calibration curve (Reimer *et al.*, 2020).

506-48/506-50 Composite depth interval	506-48/506-50 Composite mean depth	Sample weight (mg)	C weight (mg)	Radiocarbon lab. ID & Name of marker horizon	¹⁴C age BP	Calibrated age BP (IntCal20) 68.3% conf. Interval From	68.3% conf. Interval To	95.4% conf. Interval From	95.4% conf. Interval To	Median	Reference
4-5	4.5	25.7		Poz-79407	1480 ± 30	1382	1314	1400	1307	1356	Svendsen *et al.* (2019)
64-66	65	6.1		Poz-69670	2285 ± 30	2346	2184	2352	2158	2313	Svendsen *et al.* (2019)
112,5-114,5	113.5	1.3	0.3	Poz-79408	2645 ± 35	2777	2740	2848	2725	2759	Svendsen *et al.* (2019)
172-173	172.5	1.9	0.5	Poz-79409	3730 ± 35	4148	3990	4229	3934	4078	Svendsen *et al.* (2019)
209-210,5	210	105.6		Poz-69671	4565 ± 35	5320	5069	5441	5051	5225	Svendsen *et al.* (2019)
262-263	262.5	16.5	0.6	Poz-79410	5890 ± 40	6746	6664	6838	6571	6710	Svendsen *et al.* (2019)
350,5-351,5	351	77.3	0.5	Poz-69673	7750 ± 60	8590	8455	8637	8410	8520	Svendsen *et al.* (2019)
434,5-435,5	435	1.2	0.2	Poz-79412	9700 ± 70	11215	10877	11244	10780	11100	Svendsen *et al.* (2019)
469-470	469.5	5.6		Poz-79413	10010 ± 50	11686	11344	11735	11275	11500	Svendsen *et al.* (2019)
	476.5	*10.9*	*0.9*	*LuS14118*	*10250 ± 50*	*12041*	*11825*	*12442*	*11752*	*11950*	*This study*
	502.25	*1.9*	*1.0*	*LuS14119*	*10120 ± 50*	*11829*	*11507*	*11933*	*11403*	*11719*	*This study*
	511.5			Vedde Ash		12096	12008	12142	11946	12050	Haflidason *et al.* (2019) and Lohne *et al.* (2013)
	516	*8.2*	*1.0*	*LuS14120*	*10510 ± 50*	*12616*	*12480*	*12689*	*12192*	*12544*	*This study*
553	553			Beta-282484	10560 ± 50	12674	12493	12697	12480	12599	Svendsen *et al.* (2019)
	570.5	*3.0*	*0.4*	*LuS14121*	*10650 ± 65*	*12725*	*12623*	*12743*	*12491*	*12669*	*This study*
	575	*4.3*	*0.6*	*LuS14122*	*11090 ± 60*	*13091*	*12930*	*13111*	*12841*	*13004*	*This study*
	582.5	*10.0*	*1.8*	*LuS14123*	*11380 ± 60*	*13308*	*13181*	*13406*	*13122*	*13254*	*This study*
	585.5	*8.8*	*1.6*	*LuS14124*	*11410 ± 60*	*13335*	*13183*	*13420*	*13168*	*13277*	*This study*
	592.5	*1.7*	*0.2*	*LuS14125*	*11480 ± 75*	*13452*	*13300*	*13491*	*13181*	*13356*	*This study*
	627.5	*3.5*	*0.6*	*LuS14126*	*11900 ± 60*	*13804*	*13607*	*14011*	*13598*	*13754*	*This study*
635-636	635.5	12.2	2.3	Beta-473333	12310 ± 40	14770	14136	14808	14091	14256	Svendsen *et al.* (2019)
635-636	635.5	2.8	0.4	Beta-473334	12040 ± 40	14017	13809	14036	13802	13915	Svendsen *et al.* (2019)
	663.5	*2.3*	*0.4*	*LuS14127*	*12480 ± 75*	*14963*	*14453*	*15051*	*14282*	*14659*	*This study*
	674.5		*0.4*	*LuS14128*	*12520 ± 75*	*15021*	*14520*	*15117*	*14323*	*14775*	*This study*
731-733	732	6.1	2.3	Beta-282485	12700 ± 50	15230	15067	15292	14983	15145	Svendsen *et al.* (2019)
798-799	798.5	20.0		Beta-473335	13020 ± 50	15700	15512	15767	15371	15599	Svendsen *et al.* (2019)
880-882	881	*4.9*	*0.13*	*Poz-79403*	*14300 ± 140*	*17703*	*17121*	*17866*	*17055*	*17424*	Svendsen *et al.* (2019)
973-975	974		0.3	Poz-69674	14390 ± 100	17741	17391	17912	17176	17568	Svendsen *et al.* (2019)
1110,5-1114,5	1112.5	11.7	0.2	Poz-69675	15030 ± 130	18625	18212	18687	18131	18430	Svendsen *et al.* (2019)
	1153			Top varve count							Regnéll *et al.* (2019)
1183,5-1191,5	1187		0.6	Poz-69677	15660 ± 90	19010	18840	19125	18790	18933	Svendsen *et al.* (2019)
1298-1300	1299			Beta-282486	15180 ± 60	18641	18298	18661	18278	18464	Svendsen *et al.* (2019)
1544-1549	1546.5	*3.9*	*0.3*	*Poz-69678*	*17620 ± 150*	*21660*	*20988*	*21837*	*20905*	*21314*	Svendsen *et al.* (2019)
1735-1737	1736	*4.5*	*0.2*	*Poz-79414*	*17400 ± 150*	*21266*	*20833*	*21430*	*20573*	*21026*	Svendsen *et al.* (2019)
1892-1897	1894.5	*2.7*	*0.2*	*Poz-79415*	*20600 ± 210*	*25130*	*24540*	*25311*	*24193*	*24797*	Svendsen *et al.* (2019)
1892-1897	1894.5		*0.4*	*Poz-69679*	*25520 ± 270*	*30053*	*29336*	*30257*	*29185*	*29749*	Svendsen *et al.* (2019)
1946-1950	1948	*2.2*	*0.13*	*Poz-79404*	*18370 ± 210*	*22486*	*22066*	*22887*	*21871*	*22298*	Svendsen *et al.* (2019)
2065-2069	2067	*2.5*	*0.11*	*Poz-79405*	*16700 ± 170*	*20400*	*19965*	*20561*	*19621*	*20178*	Svendsen *et al.* (2019)

(Continued)

Table 1. (Continued)

| 506-48/506-50 Composite depth interval | 506-48/506-50 Composite mean depth | Sample weight (mg) | C weight (mg) | Radiocarbon lab. ID & Name of marker horizon | ^{14}C age BP | Calibrated age BP (IntCal20) | | | | | Reference |
						68.3% conf. Interval From	68.3% conf. Interval To	95.4% conf. Interval From	95.4% conf. Interval To	Median	
2352–2355	2353.5	19.8	0.7	Poz-69680	20380 ± 120	24649	24270	24913	24175	24493	Svendsen et al. (2019)
2352–2355	2353.5	3.9	0.15	Poz-79406	18750 ± 170	22875	22510	22986	22377	22685	Svendsen et al. (2019)
	2413			Base varve count							Regnéll et al. (2019)

et al., 2020). The age model of core 506-48 indicates an age of ~24 k cal a BP for the base of the core (Regnéll et al., 2019; Svendsen et al., 2019). Core 506-50 was correlated to the key core 506-48 using colour images, lamination patterns, palaeomagnetic data and XRF element analyses (Regnéll et al., 2019).

Core 506-51

To ^{14}C AMS date core 506-51, a total of 14 samples were picked for terrestrial plant fragments following the procedure described by Svendsen et al. (2019). Also in this core, the plant fragments were too small for species identification. Especially in the lower part of the core it was challenging to find enough material for dating (Eldegard, 2019) (Fig. 3). All the samples were ^{14}C dated at Beta Analytic, Florida, USA and at ETH Zürich, Switzerland (Table 2).

Results and discussion

Core lithology/stratigraphy

Core 506-48 is divided into three main lithological units. The lowermost unit C, from 11.39 m down to the bottom of the core, consists of well-defined, rhythmic layers of fine silt, interpreted to be glaciolacustrine varves (Fig. 2) (Regnéll et al., 2019; Svendsen et al., 2019). Unit B, from 6.55 to 11.39 m, is characterised by diffusely layered fine silt punctuated, with increasing frequency upwards, by thin layers of more coarse-grained turbidites. The layering and low LOI makes us interpret unit B to consist of mainly glaciolacustrine deposits. The uppermost unit A, from 6.55 m to the top, consists of massive or very diffuse layered silt, slightly coarser than that below. Unit A is frequently punctuated by 10–70 mm thick turbidites consisting of sorted fine sand and/or coarse silt. The LOI reaches the highest values within this unit. Unit A is interpreted as lacustrine sediments, not influenced by any glaciers (Fig. 2).

The lithostratigraphy in Mal. Shchuchye (core 506-51) is like Bol. Shchuchye and is similarly divided into three units as in 506-48 (Fig. 3). The lowermost unit C (8.12–25.07 m) is characterised by 1–5 mm thick, clayey-silty rhythmic layers with average grain size of 8–11 µm and LOI around 3% (Eldegard, 2019), and it is confidently correlated with unit C in core 506-48. Unit B (4.02–8.12 m) is characterised by alternating discontinuous laminated and massive layers with the mean grain size around 10–12 µm, but the LOI has dropped to 2.5% (Fig. 2c). Unit B is like unit B in core 506-48 and interpreted as a glaciolacustrine sediment. Unit A (0.00–4.02 m) consists dominantly of laminated layers frequently punctuated by 20–40 mm thick turbidite layers. LOI varies from 2.5 to 5.0%, reflecting the frequency of turbidites. The mean grain size is in general coarser than in the lower units, with coarse silt and fine sand grain size commonly found in the turbidites (Eldegard, 2019). The unit is interpreted to be lacustrine sediments, like the uppermost unit A in core 506-48 (Fig. 2).

Synthesis of the lithostratigraphy

The lithostratigraphy is very similar in all cores from both lakes. This indicates that the depositional environments are more dominated by large-scale palaeoclimatic and environmental conditions than local erosional and depositional processes associated with each basin. The large thickness of the varved units (12.6 m) in the lower part of the cores suggests stable depositional conditions that lasted for about 9.5 ka,

Table 2. Radiocarbon dates from core 506-51, Mal. Shchuchye. Dates that were not included in the final age model are marked with red letters. All ages are calibrated using the OxCal 4.4.1 software (Bronk Ramsey *et al.*, 2009a) with IntCal20 calibration curve (Reimer *et al.*, 2020)

Depth interval (cm)	Mean depth (cm)	Radiocarbon Lab ID	Conventional ¹⁴C Ages	1σ	Sample weight (mg)	Weight C (mg)	Calibrated ages (IntCal20)				
							68.3% conf. Interval From	68.3% conf. Interval To	95.4% conf. Interval From	95.4% conf. Interval To	Median
70-71	70	Beta-486108	3010	30	5.8	2.60	3320	3161	3335	3076	3203
125-126	126	Beta-486109	5040	30	11.0	2.80	5892	5734	5901	5663	5820
149-151	150	Beta-486110	7780	60	5.0	1.30	8601	8456	8721	8412	8551
247-248	248	Beta-486111	9290	30	6.0	1.90	10565	10424	10578	10306	10489
287-288	288	Beta-486112	10020	30	9.6	2.60	11681	11398	11710	11324	11512
402-404	403	Beta-486114	10990	40	6.2	2.00	12985	12831	13069	12770	12902
422-423	423	Beta-489587	11060	40	7.5	2.90	13071	12929	13092	12849	12993
473-476	474	Beta-489588	11720	40	4.2	1.60	13600	13504	13743	13480	13555
574-576	575	Beta-489589	11060	40		0.90	13071	12929	13092	12849	12993
843-846	845	Beta-489590	13020	70		0.35	15723	15479	15801	15326	15593
1307-1311	1309	ETH-89643	17362	171			21263	20755	21442	20508	20976
2388-2391	2390	Beta-489591	11220	50		2.10	13161	13100	13236	13076	13134
2410-2412	2412	Beta-489592	7500	50		1.10	8378	8211	8389	8191	8310
2459-2461	2460	ETH-89642	19656	134			23829	23389	23921	23223	23567
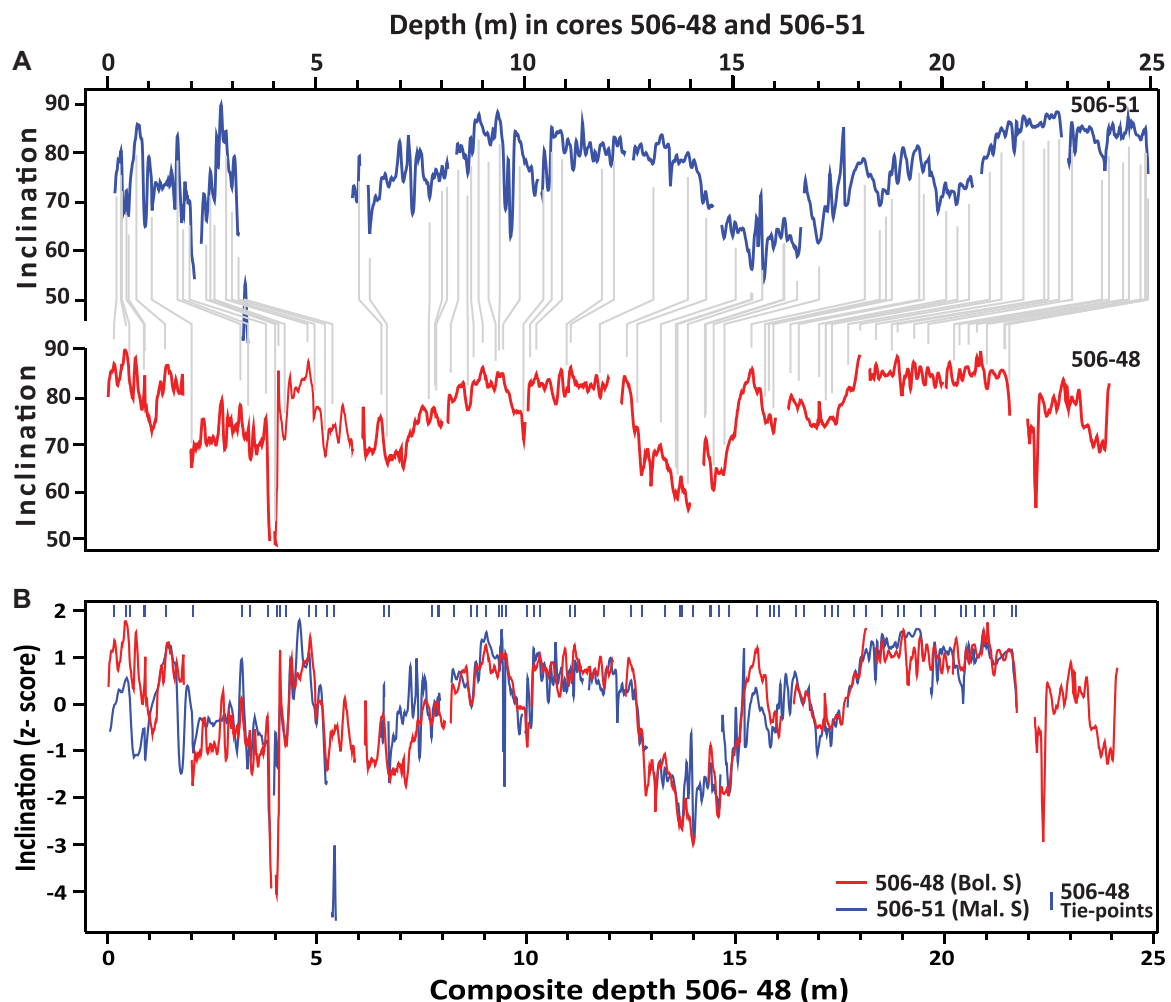
Figure 4. Correlation between the master core 506-48 from Bol. Shchuchye (red) and core 506-51 from Mal. Shchuchye (blue). A) The magnetic inclination for cores 506-48 and 506-51 plotted on their own depth scales. The grey lines show identified tie points and the correlation between the cores. B) The inclination records correlated as shown in (A) and plotted on the depth scale for core 506-48. On the *y*-axis is the inclination plotted as z-scores (standard score). Tie-point positions are marked as blue ticks on the top scale. [Color figure can be viewed at wileyonlinelibrary.com]

dominated by a high annual sediment influx from glaciers. This unit is followed by more diffuse laminations and decreasing sedimentation rates (Figs. 2 and 3), probably due to shrinking glaciers in the catchment areas (Haflidason *et al.*, 2019a;

Lenz *et al.*, 2021; Regnéll *et al.*, 2019; Svendsen *et al.*, 2019). The youngest unit is characterised by an increased frequency of turbidites and higher organic production in the lake as well as in the drainage area. During this period the catchment area
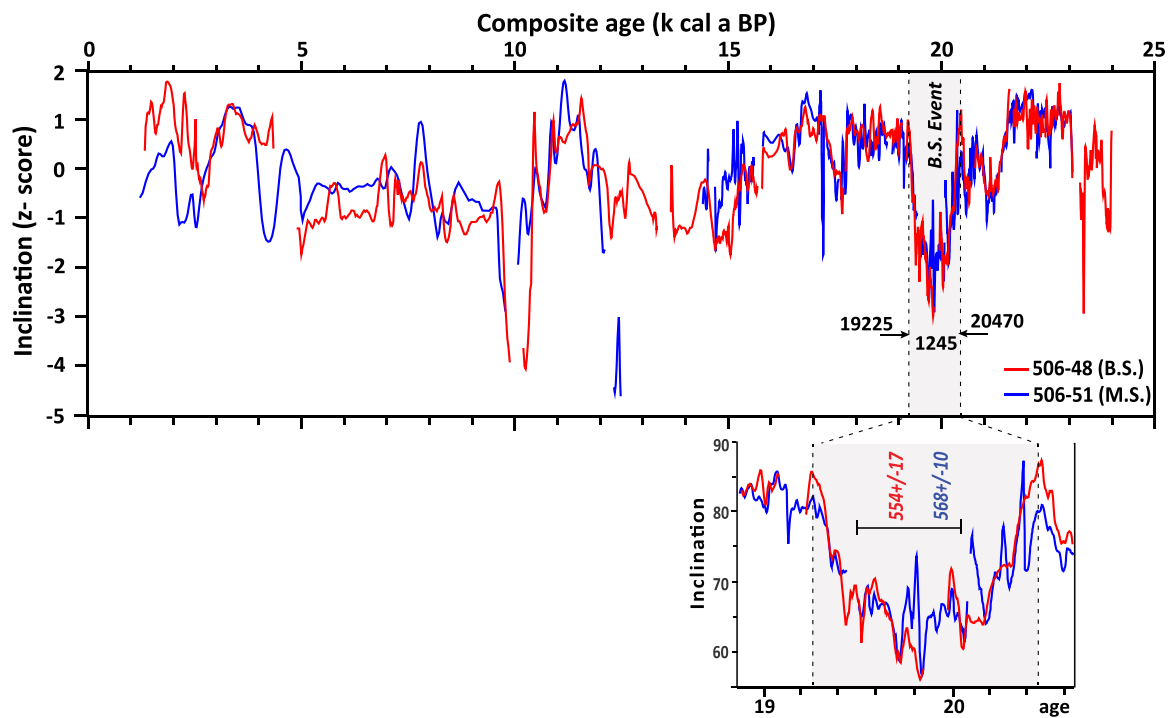
Figure 5. The inclination records from Fig. 4B (506-48 red and 506-51 blue) plotted on a linear time scale. The shaded column marks the palaeomagnetic Bol. Shchuchye Event (B.S. Event), lasting 1245 years and bracketed between 19 225 and 20 470 cal a BP. The inserted graph shows the details of the curves across the B.S. Event. The number of counted varves (colours correspond to curves) between two points identified in both cores are given with ±1σ uncertainty. [Color figure can be viewed at wileyonlinelibrary.com]

of Bol. Shchuchye became mostly ice-free, but Mal. Shchuchye may have received a small influx of glacially derived deposits at the very end of the Holocene during the little Ice Age (e.g. Haflidason *et al.*, 2019a; Lenz *et al.*, 2021; Mangerud *et al.*, 2008; Svendsen *et al.*, 2019).

Chronostratigraphy and age model for key core 506-48

In the present study we have slightly adjusted the age model of core 506-48 presented by Regnéll *et al.* (2019) and Svendsen *et al.* (2019) as we have obtained nine more ^{14}C dates (Table 1). We have changed to IntCal20 for the calibration of radiocarbon dates, and we now construct the age–depth model using the Bayesian depositional model OxCal 4.4.1 (Bronk Ramsey, 2009a) (Fig. 2) with the OxCal P_Sequence model (Bronk Ramsey, 2008). Boundary commands were inserted at the transitions between the main sediment units where there is a suspicion that the influx of sediment has changed, allowing for modelling changes in sedimentation rate at these depths. We used the variable *k* option (Bronk Ramsey and Lee, 2013) to objectively estimate how variable the sedimentation rate can be between dated samples. Each ^{14}C date was tested for being an outlier with the general outlier model (Bronk Ramsey, 2009b) assuming a prior probability of 5% for each date to be an outlier, and any resulting outliers were down-weighted in the depositional model.

The chronology of the cores was constructed in several steps. First, we constructed an age–depth model for the master core 506-48 where all ^{14}C dates and the Vedde Ash were used to model the chronology of the full core length (Fig. 2). In this stage the time intervals between ^{14}C dated samples in the varved unit C were constrained by using the varve counts (including the counting uncertainty) as an additional prior information constraint. We used the age for the Vedde Ash from Lohne *et al.* (2013), recalibrated to a median age of 12 050 cal a BP (95.4% range) using IntCal20 (Reimer *et al.*, 2020).

In the second step we substituted the chronology of the varved sequence in unit C (Regnéll *et al.*, 2019) with the actual number of varves by adding the floating varve chronology, with the associated maximum counting error (assuming that the maximum counting error represents 2σ), to the posterior probability age estimate of the unit B/C boundary (top of the varve sequence) (Table 1). This two-stage approach ensures a seamless age–depth model that is consistent with both ^{14}C dates and varve counts (Fig. 2).

We then aligned the core 506-51 to the master core 506-48 using, as the first guide to the alignment, the ^{14}C dates and stratigraphic features (e.g. presence of laminations) (Figs. 2 and 3). Aided by this guide we then defined tie points between the inclination records in stratigraphic levels where similar clear curve signals appear in all cores (Fig. 4). These tie points were then used to transfer the core 506-51 to the 506-48 depth scale by generating a depth model in OxCal, 4.4.1 for each core (Fig. 4). We assume that the error of each tie point in core 506-51 is normally distributed with a standard deviation of 2 cm. The depth-modelling approach provides a way to include uncertainty in the stratigraphic correlation which, importantly, increases between the tie points. To test the depth-model correlation, we counted the number of varves within the anomalous inclination interval at 12.5–15 m depth in core 506-48 and in the same interval in core 506-51 (Fig. 5). In this interval the laminations are well preserved in both cores and the counting, using the method described in Regnéll *et al.* (2019), gave overlapping durations of 554 ± 17 and 568 ± 10 varves in cores 506-48 and 506-51, respectively (Fig. 5).

Using the depth models, we then transferred the ^{14}C dates of core 506-51 to core 506-48 and updated the 506-48 age model with these dates, excluding some dates that were inconsistent with the inclination records. For the updated 506-48 age model we also removed from the analysis the ^{14}C dates from 506-48 that had >75% posterior probability of being an outlier. The updated chronology was then transferred
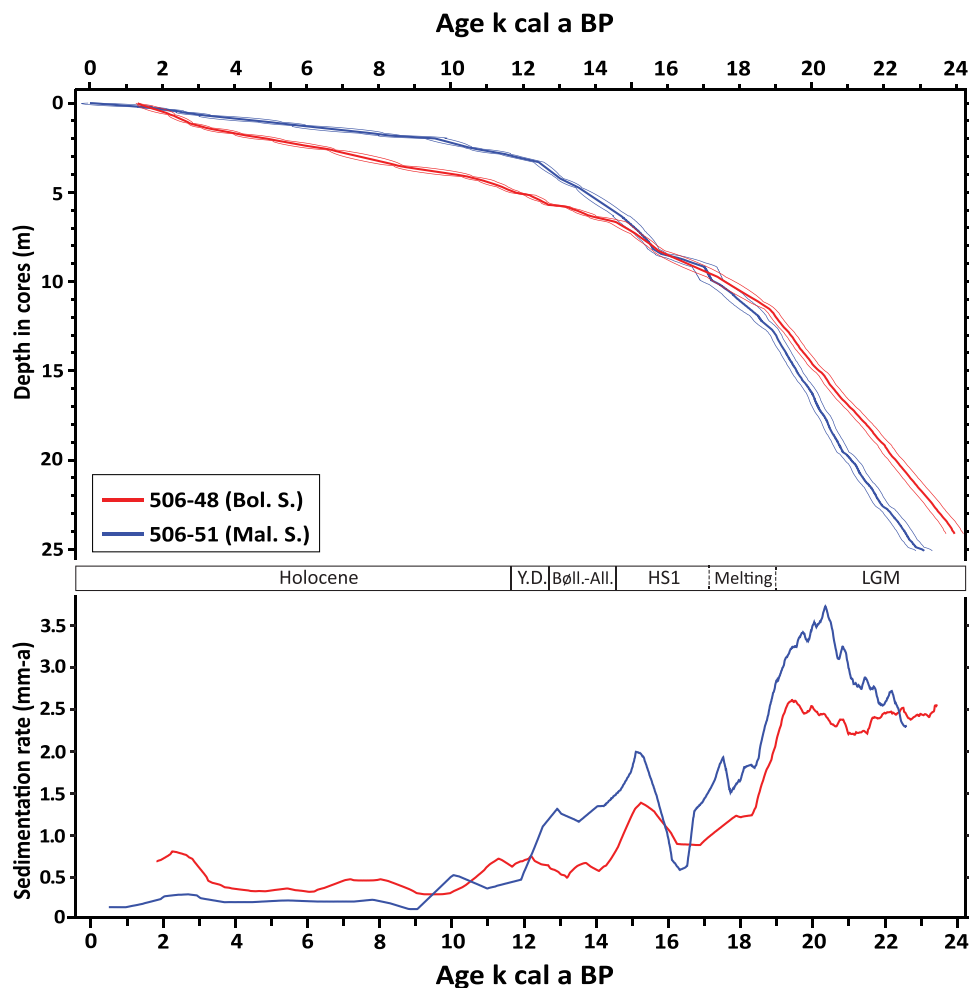
Figure 6. The upper panel shows age–depth curves for the master core 506-48 (red) from Bol. Shchuchye and core 506-51 (blue) from Mal. Shchuchye, both with a 95% confidence interval. The lower panel shows the sedimentation rate in mm a^{-1} plotted as a 1k running mean of decadal average sedimentation rates. The chronozones are marked as in Fig. 2. [Color figure can be viewed at wileyonlinelibrary.com]

back to core 506-51. The age uncertainty associated with the depth models was propagated into the age model by taking the root sum of squared standard deviations. See supplementary text for the full details of the age-model construction.

Evaluation of the ^{14}C ages

The depositional age models for both the Bol. and the Mal. Shchuchye cores is considered to be precise for the Holocene period although most of the ^{14}C ages are based on small plant fragments or macrofossils (Figs. 2 and 3; Tables 1 and 2). The amount of plant fragments within the Holocene part of the cores is much larger, and gives better confidence in the dating results, than in the deeper parts of the cores.

The amount of datable material in samples from the deeper part of the cores is generally at the minimum limit to be AMS ^{14}C dated. To reduce the potential risk of laboratory contamination all the samples selected for ^{14}C dating were routinely picked in a clean air-filtered cabin before delivery to the ^{14}C dating laboratories. Another potential source of dating error is contamination from plant fragments reworked from old terrestrial strata. This was particularly evaluated in core 506-48 by dating and analysing a large number of samples. An important test showed a perfect match between the obtained ^{14}C ages and the age of the Vedde Ash horizon (Haflidason et al., 2019b). In the lowermost part of the core a count of >5000 continuous varves made it possible to create an internal age control confirming the age range of the established age model for the oldest part of the core

stratigraphy (Regnéll et al., 2019). To evaluate the consistency of the down-core pattern of the dating results a Bayesian statistical model was run using all the dating points available from core 506-48. The final results demonstrate that the down-core consistency is internally very high with only a few identified outliers (Fig. 2).

The palaeomagnetic secular variations and their importance for correlation and dating

The stable influx of fine-grained sediments seems to have favoured the preservation of the magnetic signal in the lake sediments. This is supported by the fact that the palaeomagnetic inclination plots show nearly identical palaeomagnetic secular variations (PSV) in all the studied cores (Figs. 2, 3, 4, 5 and S1) as well in core Co1321 from Lake Bol. Shchuchye (Lenz et al., 2021). As an example, the distinct geomagnetic deviation at 12.5–15.0 m depth in core 506-48 (about 20 k cal a BP) is reproduced even down to the smallest details in the other cores studied (Figs. 4, 5 and S1). The similar rate and pattern of the sedimentation rate found within both the studied lakes (Fig. 6) also contributes to verification of the matching age models for the PSV records in both lakes. Further, the high quality of the ChRM directions record in cores 506-48/50 results from a homogeneous magnetic mineralogy with a strong remanent magnetisation (10^{-2} A/m), constant magnetic susceptibility between 2×10^{-5} and 12×10^{-5} in the Holocene part of the core and $15–23 \times 10^{-5}$ for the pre-Holocene part (Fig. S1) demonstrating a stable influx of magnetic minerals.

The PSV record for core 506-48 represents a high-resolution PSV pattern covering a continuous period spanning the last 24 ka. The fact that the same PSV pattern has been reproduced in such high detail in several cores from two lakes indicates that it also has the potential to be used in other marine and lake records, even where the resolution is considerably lower.

We name this event at 19 225–20 470 cal a BP (lasting 1245 yrs) the Bol. Shchuchye Event. Several palaeo-intensity and palaeomagnetic directional events have during the last two to three decades been described and dated to have occurred within the time interval 17–22 ka (e.g. Muscheler *et al.*, 2005; Nowaczyk *et al.*, 2013; Singer *et al.*, 2014 and references therein; Channell *et al.*, 2018; Nawrocki *et al.*, 2018; Reilly *et al.*, 2018; Lenz *et al.*, 2021). However, as these events are found in stratigraphically fragmentary or low-resolution records, this palaeomagnetic event has previously not been fully explored or documented. In the present study only the inclination record is presented and used as a correlation tool for our closely spaced lake records. A more thorough palaeomagnetic study on the full palaeomagnetic data set is in progress, including a full discussion on long-distance correlations.

Palaeoenvironmental implications

The synchronised age models and sedimentation rate records for the Bol. Shchuchye and the Mal. Shchuchye lakes give a good overview over the development in the sediment flux into the lakes for the last ~24 ka (Figs. 1 and 6). The records in the two lakes follow the same pattern with the highest sedimentation rate during the LGM, followed by a rapid drop (~50%) during the early melting phase period, and a rapid increase at the end of stage HS1 and into the Bølling–Allerød. From the middle of the Younger Dryas and through the Holocene the sedimentation rate is generally stable but low, only affected by minor fluctuations.

The sedimentation-rate values give a good documentation of how the sediment flux into the lakes has varied since the peak of LGM and to the present even though they represent only the coring sites. The fact that the sedimentation pattern is found to be almost similar through the last ~24 ka means that both lake areas have been exposed to similar glacial and environmental conditions since the peak of the LGM (Svendsen *et al.* 2019).

Conclusions

- Detailed age models covering the last ~24 k cal a BP have been developed for the stratigraphy in the lakes Bol. Shchuchye and Mal. Shchuchye in the Polar Ural Mountains, Russia.
- The palaeomagnetic inclination curves show nearly identical PSV in all core records from both lakes, demonstrating that both lakes have experienced similar dispositional history.
- A large and very distinct inclination deviation, named the Bol. Shchuchye Event, was identified in all cores retrieved from both lakes. It lasted over a period of 1245 years, from 20 470 to 19 225 cal a BP. We expect it to be crucial for correlations.
- The well-dated and reproducible palaeomagnetic inclination graph offers a new possibility to correlate archives in the Arctic for the last ~24 k cal a BP, probably also over a long distance.
- We demonstrate the importance of using several dating methods associated with an internal age control to establish a reliable and robust age model.

- The sedimentation rate shows the same trend in all cores from both lakes, including high input during the LGM and gradually lowering after ~18 k cal a BP to low stable Holocene values.

Supporting information

Additional supporting information can be found in the online version of this article.

Figure S1. Inclination and the magnetic susceptibility records from cores 506-48 and 506-50 plotted on their common depth scale. Both these palaeomagnetic parameters are reproduced in detail in both cores. The cores are located 20 m apart, but with an overlap of ~30–40 cm between each core segment.

Figure S2. Core depth correlation plot showing the tie points on the inclination curves in core 506-51 that were used to link that core with the well-dated key core 506-48 (Fig. 4). These tie points are important input to develop a refined age model for core 506-51.

Figure S3. Flow diagram outlining the processes applied to produce the final age models for the cores.

Figure S4. A) The one-sigma uncertainty in the age models for core 506-51. The total uncertainty is calculated as the sum of the square root of the sum of squares of the 506-48 age model uncertainties and the depth model uncertainties of core 506-51. B) The graphs show the total uncertainty of the transferred age models for core 506-51 together with the uncertainty of the final models. In the final age model, we have used ^{14}C dates from the individual cores together with tie-point ages from the inclination correlation to the key core 506-48 for the Holocene and the late glacial period. The final modelling step improved the precision of the 506-51 age model for the last 15 ka on average with 39 years (1σ) or 23% compared with the primary data set. Results of this refining of the 506-51 age model is illustrated in Fig. S5.

Figure S5. Plot of core 506-51 illustrating the refinements of the age model following the procedure described in Figs S3 and S4. The age model for core 506-51 covering the last 13–14 k cal a BP is plotted as the mean ±2σ ranges, both for the transferred age and the final age model. Note that while the precision is considerably improved, there is no real difference in the mean values of the age model.

Table S1. The age model for the master core 506-48. Model ages (mean, median and ±2 standard deviations) and inclination values are listed along with depth in the master core.

Table S2. The age model for core 506-51 with mean, median and ±2 standard deviations.

Supporting information.

ORCID

Haflidi Haflidason http://orcid.org/0000-0002-7782-8856
Jo Brendryen http://orcid.org/0000-0002-5825-0518
Carl Regnéll http://orcid.org/0000-0002-5662-4950
John Inge Svendsen http://orcid.org/0000-0002-0570-466X

References

Alexanderson H, Backman J, Cronin TM *et al.* 2014. An Arctic perspective on dating Mid-Late Pleistocene environmental history. *Quaternary Science Reviews* **92**: 9–31.

Bjune AE, Alsos IG, Brendryen J *et al.* 2021. Rapid climate changes during the Late glacial and the early Holocene– as seen from plant community dynamics in the Polar Urals, Russia. *Journal of Quaternary Science* (this issue)

Blott SJ, Pyne K. 2001. GRADISTAT: a grain size distribution and statistics package for the analysis of unconsolidated sediments. *Earth Surface Processes and Landforms* **26**: 1237–1248.

Bronk Ramsey C. 2008. Deposition models for chronological records. *Quaternary Science Reviews* **27**: 42–60.

Bronk Ramsey C. 2009a. Bayesian analysis of radiocarbon dates. *Radiocarbon* **51**: 337–360.

Bronk Ramsey C. 2009b. Dealing with outliers and offsets in radiocarbon dating. *Radiocarbon* **51**: 1023–1045.

Bronk Ramsey C, Lee S. 2013. Recent and Planned Developments of the Program OxCal. *Radiocarbon* **552**: 720–730.

Channell JET, Hodell DA, Crowhusrt SJ *et al.* 2018. Relative paleointensity (RPI) in the latest Pleistocene (10-45 ka) and implications for deglacial atmospheric radiocarbon. *Quaternary Science Reviews* **191**: 57–72.

Clark CL, Edwards ME, Gielly L *et al.* 2019. Persistence of arctic-alpine flora during 24,000 years of environmental change in the Polar Urals. *Scientific Reports* **9**: 19613.

Clarke CL, Alsos IG, Edwards ME *et al.* 2020. A 24,000-year ancient DNA and pollen record from the Polar Urals reveals temporal dynamics of arctic and boreal plant communities. *Quaternary Science Reviews* **247**: 106564.

Colman SM, Jones GA, Rubin M *et al.* 1996. AMS radiocarbon analyses from Lake Baikal, Siberia: challenges of dating sediments from a large, oligotrophic lake. *Quaternary Science Reviews* **15**: 669–684.

Cowling OC, Thomas EK, Svendsen JI *et al.* 2021. The Polar Ural Mountains experienced rapid shifts in moisture source and summer water balance during the last deglaciation and early Holocene. *Journal of Quaternary Science* (this issue)

Dean WE. 1974. Determination of carbonate and organic matter in calcareous sediments and sedimentary rocks by loss on ignition: comparison with other methods. *Journal of Sedimentary Petrology* **44**: 242–258.

Dushin VA, Serdyukova OP, Malyugin AA *et al.* 2009. State Geological Map of the Russian Federation 1:200000.Polar Ural Series. Sheet Q-42-I, II (Laborovaya). VSEGEI: St. Petersburg (in Russian).

Eldegard RF. 2019. Glasiasjons- og klimahistorie de siste 22 000 år, basert på sedimentstratigrafi i Maloya Shchuchye, Polar Ural, Russland. MSc thesis, University of Bergen.

Gromig R, Lebas E, Savelieva L *et al.* 2021. Sedimentation history of lake taymyr, central russian arctic, since the last glacial maximum. *Journal of Quaternary Science* (this issue). https://doi.org/10.1002/jqs.3342

Gromig R, Wagner B, Wennrich V *et al.* 2019. Deglaciation history of Lake Ladoga (northwestern Russia) based on varved sediments. *Boreas* **48**: 330–348.

Haflidason H, Zweidorff JL, Baumer M *et al.* 2019a. The Lastglacial and Holocene Seismostratigraphy and sediment distribution of Lake Bolshoye Shchuchye, Polar Ural Mountains, Arctic Russia. *Boreas* **48**: 452–469.

Haflidason H, Regnell C, Pyne-O'Donnell S *et al.* 2019b. Extending the known distribution of the Vedde Ash into Siberia: Occurrence in lake sediments from the Timan Ridge and the Ural Mountains, northern Russia. *Boreas* **48**: 444–451.

Heiri O, Lotter AF, Lemcke G. 2001. Loss on ignition as a method for estimating organic and carbonate content in sediments: reproducibility and comparability of results. *Journal of Paleolimnology* **25**: 101–110.

Henriksen M, Mangerud J, Matiouchkov A *et al.* 2008. Intriguing climatic shifts in a 90 kyr old lake record from northern Russia. *Boreas* **37**: 20–37.

Hodell DA, Nicholl JA, Bontognali TRR *et al.* 2017. Anatomy of Heinrick Layer 1 and its role in the last deglaciation. *Paleoceanography* **32**(2): 284–303.

Hovland MN 2015. Innsjøsedimentasjon og klimautvikling i de polare Uralfjellene. MSc thesis, University of Bergen.

Hughes AL, Gyllencreutz R, Lohne ØS *et al.* 2016. The last Eurasian ice sheets – a chronological database and time-slice reconstruction, DATED-1. *Boreas* **45**: 1–45.

Lammers Y, Clarke C, Erséus C *et al.* 2019. Clitellate worms (Annelida) in late-glacial and Holocene sedimentary DNA records from the Polar Urals and northern Norway. *Boreas* **48**: 317–329.

Lenz MM, Andreev A, Nazarova L *et al.* 2021. Climatic and environmental history of the Polar Ural Mountains since early MIS 2 inferred from a 54-m-long sediment core from Lake Bolshoye Shuchye. *Journal of Quaternary Science* (this issue)

Lohne ØS, Mangerud J, Birks HH. 2013. IntCal13 calibrated ages of the Vedde and Saksunarvatn ashes and the Younger Dryas boundaries from Kråkenes, western Norway. *Journal of Quaternary Science* **29**: 506–507.

Mangerud J, Gosse J, Matiouchkov A *et al.* 2008. Glaciers in the Polar Urals, Russia, were not much larger during the Last Global Glacial Maximum than today. *Quaternary Science Reviews* **27**: 1047–1057.

Mangerud J. 2021. The discovery of the Younger Dryas, and comments on the current meaning and usage of the term. *Boreas* **50**: 1–5.

Muscheler R, Burg J, Kubik PW *et al.* 2005. Geomagnetic field intensity during the last 60,000 years based on ^{10}Be and ^{36}Cl from the Summit ice cores and ^{14}C. *Quaternary Science Reviews* **24**: 1849–1860.

Nawrocki J, Bogucki A, Łanczont M *et al.* 2018. The Hilina Pali palaeomagnetic excursion and possible self-reversal in the loess from western Ukraine. *Boreas* **47**: 954–966.

Nowaczyk NR, Frank U, Kind J *et al.* 2013. A high-resolution paleointensity stack of the past 14 to 68 ka from Black Sea sediments. *Earth Planetary Science Letters* **384**: 1–16.

Oda H, Xuan C. 2014. Deconvolution of continuous paleomagnetic data from pass-through magnetometer: A new algorithm to restore geomagnetic and environmental information based on realistic optimization. *Geochemistry, Geophysics, Geosystems* **15**: 3907–3924.

Oda H, Xuan C, Yamamoto Y. 2016. Toward robust deconvolution of pass-through paleomagnetic measurements: new tool to estimate magnetometer sensor response and laser interferometry of sample positioning accuracy. *Earth Planets and Space* **68**: 109.

Puchkov VN. 1997. Structure and geodynamics of the Uralian orogeny. Orogeny through time. *Geological Society, London, Special Publications* **121**: 201–234.

Regnéll C, Haflidason H, Mangerud J *et al.* 2019. A Glacial and climate history of the last 24 000 years in the Polar Ural Mountains, Arctic Russia, inferred from partly varved lake sediments. *Boreas* **48**: 432–443.

Reilly BT, Stoner JS, Hatfield RG *et al.* 2018. Regionally consistent Western North America paleomagnetic directions from 15 to 35 ka: Assessing chronology and uncertainty with paleosecular variation (PSV) stratigraphy. *Quaternary Science Reviews* **201**: 186–205.

Reimer PJ, Austin WEN, Bard E *et al.* 2020. The IntCal20 northern hemisphere radiocarbon age calibration curve (0-55 cal kBP). *Radiocarbon* **62**: 725–757.

Roberts AP. 2006. High-resolution magnetic analysis of sediment cores: Strengths, limitations and strategies for maximizing the value of long-core magnetic data. *Physical Earth Planetary International* **156**: 162–178.

Saarnisto M, Saarinen T. 2001. Deglaciation chronology of the Scandinavian Ice Sheet from the Lake Onega Basin to the Salpausselkä End Moraines. *Global and Planetary Change* **31**: 387–405.

Singer BS, Jicha BR, He H *et al.* 2014. Geomagnetic field excursion recorded 17 ka at Tianchi Volcano, China: new ^{40}Ar/^{39}Ar age and significance. *Geophysical Research Letters* **41**: 2794–2802.

Svendsen JI, Alexanderson H, Astakhov VI *et al.* 2004. Late Quaternary ice sheet history of Northern Eurasia. *Quaternary Science Reviews* **23**: 1229–1271.

Svendsen JI, Krüger LC, Mangerud J *et al.* 2014. Glacial and vegetation history of the Polar Ural Mountains in northern Russia during the Last Ice Age, Marine Isotope Stages 5-2. *Quaternary Science Reviews* **92**: 409–428.

Svendsen JI, Færseth LMB, Gyllencreutz R *et al.* 2019. Glacial and environmental changes over the last 60 000 years in the Polar Ural Mountains, Arctic Russia, inferred from a high resolution lake record and other observations from adjacent areas. *Boreas* **48**: 407–431.

Vyse SA, Herzschuh U, Andreev AA *et al.* 2020. Geochemical and sedimentological responses of arctic glacial Lake Ilirney, chukotka (far east Russia) to palaeoenvironmental change since ~51.8 ka BP. *Quaternary Science Reviews* **247**: 9–31.

Weeks RJ, Laj C, Endignoux L *et al.* 1993. Improvements on long core measurement techniques: applications in palaeomagnetism and palaeoceanography. *Geophysical Journal International* **114**: 651–662.